Unexpected metabolic disorders induced by endocrine disruptors in Xenopus tropicalis provide new lead for understanding amphibian decline

Christophe Regnault, Marie Usal, Sylvie Veyrenc, Karine Couturier, Cécile Batandier, Anne-Laure Bulteau, David Lejon, Alexandre Sapin, Bruno Combourieu, Maud Chetiveaux, et al.

An unexpected metabolic syndrome induced by endocrine disruptors in *Xenopus tropicalis*: a new lead for understanding amphibian decline

Short title: Metabolic defects and endocrine disruptors in frogs

Christophe Regnault[a1], Marie Usal[a1], Sylvie Veyrenc[a], Karine Couturier[b], Cécile Batandier[b], Anne-Laure Bulteau[c], David Lejon[d], Alexandre Sapin[d], Bruno Combourieu[d], Maud Chetiveaux[e], Le May Cédric[e], Lafond Thomas[f], Muriel Raveton[a] and Stéphane Reynaud[a2].

[a] Univ. Grenoble-Alpes, CNRS, LECA, 38000 Grenoble, France.

[b] Univ. Grenoble-Alpes, INSERM, LBFA, 38000 Grenoble, France.

[c] Institut de Génomique Fonctionnelle de Lyon, Univ. Lyon 1, CNRS UMR5242, Ecole Normale Supérieure de Lyon, 69000 Lyon, France.

[d] Rovaltain Research Company, F26300 Alixan, France

[e] Plate-forme Therassay, l'institut du thorax, INSERM, CNRS, Univ. Nantes, Nantes, France.

[f] Centre de Ressources Biologiques Xénopes, Univ. Rennes 1, CNRS, UMS 3387, Rennes France.

[1] Contribute equally to the work

[2] To whom correspondence should be addressed.

Email addresses: CR: christophe.regnault@gmail.com, MU: marie.usal@hotmail.fr, SV: sylvie.veyrenc@univ-grenoble-alpes.fr, KC: karine.couturier@univ-grenoble-alpes.fr, CB : cecile.batandier@univ-grenoble-alpes.fr, ALB: anne-laure.bulteau@ens-lyon.fr, DL: dlejon@rovaltainresearch.com, AS: asapin@rovaltainresearch.com, BC: bcombourieu@rovaltainresearch.com, MC: maud.chetiveaux@univ-nantes.fr, CLM:

cedric.lemay@univ-nantes.fr, TL, thomas.lafond@univ-rennes1.fr, MR: muriel.raveton@univ-grenoble-alpes.fr, SR: stephane.reynaud@univ-grenoble-alpes.fr

Abstract

Despite numerous studies suggesting that amphibians are highly sensitive to endocrine disruptors (ED) their role in the decline of populations and the underlying mechanisms remain unclear. This study showed that frogs exposed to ED throughout their life cycle, at concentrations within the limits for safe drinking water, developed a prediabetes phenotype and, more generally, a global metabolic syndrome. Female *Xenopus tropicalis* exposed to benzo[a]pyrene and triclosan (50 $ng.L^{-1}$) from the tadpole stage displayed glucose intolerance syndrome, liver steatosis, liver mitochondrial dysfunction, liver transcriptomic signature and pancreatic insulin hyper secretion typical of a pre-diabetes state. This metabolic syndrome was associated with delayed metamorphosis along with decreased size and weight at metamorphosis in their progeny, which has been linked to reduced adult recruitment and likelihood of reproduction. Indeed, F1 animals displayed a decrease in their reproductive success demonstrating decreased fitness in ED-exposed xenopus. Moreover, after one year of depuration, xenopus exposed to benzo[a]pyrene still displayed hepatic disorders and a marked insulin secretory defect resulting in glucose intolerance. Our results demonstrate that amphibians are highly sensitive to ED at concentrations not reported as inducing stress in other vertebrates. This study constitutes a starting point for considering ED as one of the key contributing factors of the amphibian population decline, through their disruption of energetic metabolism. From a broader perspective, our results show that ED cause metabolic disorders and confirm epidemiological studies suggesting that environmental ED might account for a substantial proportion of the incidence of metabolic diseases in humans.

Keywords: endocrine disruptors**,** metabolic syndrome, amphibian population decline, transgenerational, *Xenopus tropicalis*

Significance Statement

By performing a controlled exposure of an amphibian model to endocrine disruptors (ED) at concentrations within the range of safe drinking water, we provide the first evidence of the role these widespread contaminants play in amphibian population decline through metabolic disruption. In frogs exposed throughout their life cycle this disruption induces a spectacular metabolic syndrome characteristic of a pre-diabetes state. Exposed animals produce progeny with a time delay to metamorphosis, smaller size and weight at the adult stage, and which have reduced reproductive success. These transgenerational impacts of ED may have very serious consequences in terms of overwintering survival, recruitment for reproduction, and fitness which constitute the starting point for population decline.

Introduction

Dramatic declines in amphibian populations in wetlands have been described worldwide since the 1980s (1), with current extinction rates reaching levels that are 211 times higher than background levels (2). It has been suggested that multiple pollution of wetlands by endocrine disruptors (ED) plays a key role, together with other well-known threats including habitat loss, the introduction of exotic species, increased UV radiation, water acidification, and emerging infectious diseases (3-5). Some field studies using landscape-scale data have suggested that ED may correlate with population decline in several amphibian species. Therefore, it was suggested that contamination by ED is one of the key contributing factors responsible for altering amphibian population fitness (6). However, despite evidence suggesting that when the first symptoms of ED toxicity arise in an amphibian population it is often too late to stop the destructuring of the community and the population decline processes (3), the role of ED in this phenomenon has been called into question by a number of researchers who have suggested that amphibians are no more vulnerable to ED than other species (7). ED have been extensively studied in vertebrates, focusing on their capacity to interfere with reproductive development and sex differentiation. Exposure to ED at the larval stage can disrupt organogenesis and gonadal differentiation (8-14) by acting on thyroid and reproductive axes crosstalk (15). Another sensitive phase is the breeding season during which exposure of adult frogs to ED at critical phases can lead to egg and sperm maturation defects (16-24). In addition to these developmental and reproductive effects, there are also growing concerns that metabolic disorders might be linked with ED (25). Data from epidemiological studies suggest that environmental ED might account for a substantial proportion of the incidence of metabolic diseases in humans (26-28). Despite these epidemiological correlations and experimental evidence in mammals (29-31), the potential involvement of ED in metabolic disorders as a possible cause of a reduction in fitness in amphibians has been largely neglected. Recent studies did demonstrate that acute exposure to

benzo[a]pyrene (BaP) and triclosan (TCS) can induce marked metabolic disorders in female and male *Xenopus tropicalis* with an insulin resistance-like (IR) syndrome phenotype and hepatotoxicity due to impaired lipid metabolism (32, 33). However, the precise impact of ED, at concentrations typically found in aquatic ecosystems, on metabolism and the subsequent consequences on amphibian health and their decline is unknown.

Here we reveal the real impact of ED on amphibian metabolism and their consequences in terms of fitness by studying two widespread ED, BaP and TCS, at environmental concentrations (34, 35) in the range of safe drinking water (36, 37). Exposing female *Xenopus* from tadpole to mature adult stage (12 month) to BaP and TCS at 50 $ng.L^{-1}$ led to a hepatic transcriptomic signature and liver, muscle, and pancreatic physiological impairments typical of a pre-diabetes state. For BaP exposure, the observed metabolic syndrome was irreversible after one year of depuration in clean water. Thus, by testing the relationship between ED exposure and fitness we observed that exposed animals displayed a dramatic decrease in reproductive success and produced progeny (F1) with a decreased capacity to reproduce and produce viable progeny (F2). These data suggest that ED may have a direct causal relationship to amphibian population decline by disrupting energetic metabolism, and provide new insights into their transgenerational effects.

Results and Discussion

Development of ED-exposed animals (F0)

BaP and TCS-exposed animals showed a significant time delay to metamorphosis (21 and 31 days longer to reach 90% frog metamorphosis in the population (Fig. S1a) but no significant decrease in their size and weight at metamorphosis was observed (Fig. S1b-c). Moreover,

regardless of the ED considered, no difference in the time delay to achieve sexual maturity was observed in exposed females (Fig. S1d).

ED induce a marked metabolic syndrome in *Xenopus* typical of a pre-diabetes state

No difference in basal serum glucose levels was found between the exposed and control animals. However, ED exposure led to a reduction in glucose tolerance with a 2.4 to 1.8 fold increase in blood glucose (Fig. 1a). Investigating the physiology of the liver showed that the ED-exposed animals which had become glucose intolerant displayed a marked increase in their hepatosomatic index, correlated with marked hepatic steatosis (Fig. 1b-c). This deregulation of lipid metabolism in the liver was associated with marked hypertriglyceridemia (Fig. 1d). Mitochondria orchestrate energy metabolism from lipids through substrate oxidation via β-oxidation (38) and mitochondrial dysfunction has been associated with chronic liver steatosis (29). Here we showed a mitochondrial uncoupling in exposed animals highlighted by an increase in the State 2 respiratory rate and a decrease of respiratory control index (RCI) (Fig 1 e,f). Fatty liver and mitochondria uncoupling has been associated with oxidative stress (38). A general deficit of Fe-S cluster proteins, such as *aconitase*, a tricarboxylic acid cycle mitochondrial enzyme that contains a 4F–4S cluster as prosthetic group, is a phenotype commonly associated with oxidative stress in the mitochondria (39). Our results suggest that ED exposure induces increased rates of free radical production by the mitochondria that result in aconitase inactivation (Fig. 1g). In addition, since citrate synthase activity remained stable regardless of the treatment considered (Fig. 1h), the changes in mitochondrial parameters described above were not associated with variations in mitochondrial density in the liver. Taken together, our results suggest that liver steatosis induced by ED is linked to mitochondrial dysfunction, and specifically to mitochondrial uncoupling associated with oxidative stress.

Liver lipid accumulation has been also widely associated with hepatoxicity (40). ED-exposed *Xenopus* displayed a 2.8 to 3.2 increase in serum activity of alanine aminotransferase (ALAT; Fig. 1i) and liver necrosis associated with pronounced tissue disorganization. Under magnification, the liver tissue in exposed *Xenopus* showed hepatocytes with fewer cell contacts and irregular shapes together with large areas of necrosis (Fig. 1j-o). Proteasome dysregulation has been associated with endoplasmic reticulum (ER) stress and is the primary event of insulin resistance development (41). Here we found that ED exposure induced a 2-fold decrease in liver proteasome activity (Fig. 1 p) suggesting that general insulin resistance syndromes occur regardless of the pollutant studied. This development of insulin resistance syndrome in ED-exposed *Xenopus* is supported by the 2-fold increase in insulin production by the pancreatic beta cells (Fig.1q). In type 2 prediabetes, an increased metabolic demand for insulin due to insulin resistance precedes the onset of hyperglycemia. There is therefore a period of normal glycaemia, during which the pancreatic β cells compensate for insulin resistance through the hypersecretion of insulin (42). Nonalcoholic fatty liver disease (NAFLD) and its progression to nonalcoholic steatohepatitis (NASH) are hepatic signs of metabolic disorders including prediabetes and insulin resistance syndrome. Histological modifications associated with NAFLD/NASH include steatosis, inflammation, hepatocellular ballooning and fibrosis (43). Liver sections of ED-exposed animals presented severe steatosis, leucocyte infiltrates, and hepatocyte ballooning, especially in BaP-treated animals (Fig. 1k, n). TCS-exposed animals displayed swollen blood vessels typical of NAFLD (44) (Fig. 1o). The severity of the histopathological phenotypes observed suggests that TCS-exposed animals presented livers with modifications typical of NAFLD and that BaP-exposed *Xenopus* presented livers with modifications typical of progression to NASH. However, regardless of the liver sections considered, and despite the large areas of necrosis, no fibrosis was observed in BaP-exposed frogs (Fig. 1k). In addition to the liver, pancreatic and blood phenotypes, we also observed a marked decrease in muscle glycogen contents for ED-exposed animals (Fig. 1r) suggesting an

insulin resistance syndrome in the skeletal muscle (45). Taken together, our results suggest that ED exposure may lead to a prediabetes phenotype and more generally to the development of large metabolic syndrome in frogs exposed throughout their life cycle. Moreover, we observed a marked increase in the liver glycogen content in BaP-exposed animals (Fig. 1s). These results highlight that the metabolic syndrome observed with this compound is associated with a glycogenic hepatopathy which has been described in humans as a complication of uncontrolled diabetes (46).

Liver transcriptomic signatures in ED-exposed animals confirm the metabolic syndrome

Liver transcriptomes of ED-exposed animals highlighted the differential transcription of 322 and 121 genes for BaP and TCS, of which 40 and 66 % were up regulated, respectively (Tables S1 and S2). Interestingly, despite having a similar prediabetes phenotype, the liver transcriptomic signatures varied for different treatments. KEGG pathway enrichment analyses performed on the differentially transcribed genes indicate a link between BaP treatment and “Metabolic pathways” (2.9-fold), “Biosynthesis of amino acids” (3.5-fold), “Steroid hormone biosynthesis” (3.7-fold); “Peroxisome” (3.7-fold), “Chemical carcinogenesis” (3.8-fold); “Carbon metabolism” (3.8-fold); “Metabolism of xenobiotics by cytochrome P450” (4.1-fold); “Glycine, serine and threonine metabolism” (7.8-fold); “Glyoxylate and dicarboxylate metabolism” (8-fold); “Protein export” (13.2-fold) and “Protein processing in endoplasmic reticulum” (5.4-fold) (Fig. 2a). For TCS exposure a significant enrichment was observed for “FoxO signaling pathway” (3.7-fold); “Protein processing in endoplasmic reticulum” (3.4-fold) “Metabolism of xenobiotics by cytochrome P450” (7.4-fold) and “Chemical carcinogenesis” (7.1-fold) (Fig. 2a). Interestingly, the “Metabolism of xenobiotic by cytochrome P450” and “Chemical carcinogenesis” pathway enrichment found for both ED do not correlate with the differential transcriptions of genes involved in BaP and TCS

metabolism or bioactivation. This suggests that frogs' strategy for xenobiotic protection is not linked with the induction of biotransformation activities (32, 33) (Fig 2b and Tables S1 and S2).

Chronic ER stress due to the accumulation of unfolded proteins in the liver has been described in various models of NAFLD (47). Here we found a marked enrichment of the pathways linked to protein processing and export, highlighted by a decrease in ED-exposed animals in the transcription of genes coding for proteins involved in adaptive unfolded protein response (UPR) (*hspa5, dnajc3, dnajc9, dnajb9, dnajb11, pdia4, hsp90b1, calr,* Fig2.c, e and Tables S1 and S2). Since ER stress has been linked to the inhibition proteasome activity (41) these results suggest that the adaptive UPR response was inhibited by ED exposure in frogs. This type of inhibition has been linked to cell death (48) and explains the large areas of necrosis observed in the liver sections of BaP-exposed animals (Fig. 1k).

The other pathways found to be enriched must be considered as a whole and suggest that an IR phenotype occurs in *X. tropicalis* exposed to ED. These pathways mainly encompass genes linked to carbohydrate or lipid metabolism (Fig 2b, d). In addition, we found several other differentially transcribed genes for which a deregulation has also been associated with IR and NAFLD/NASH (Fig 2e). IR is characterized by an increase in the enzyme-coding transcripts involved in gluconeogenesis, such as *glucose-6 phosphatase* (*g6pc*) or *glyoxylate reductase* (*grhpr.1*) (49, 50). Indeed, we found a marked overtranscription of the *g6pc* (6.8-fold for BaP and 2.5-fold for TCS) and *grh.1* (2.6-fold for BaP) genes. Moreover, the high overtranscription of the *insulin-like growth factor 1 binding protein* (*igfbp-1*) repressed by insulin in physiological conditions (51) confirmed this phenotype for BaP-exposed *Xenopus* (Fig. 2b, e). The high activation of gluconeogenesis in BaP-exposed animals might be related to the high overtranscription of the nuclear receptors *nr4a1* (6.7-fold) and *nr4a2* (14-fold) which are key activators of glucose production in the liver (52) (Fig. 2 e).

IR syndrome has also been associated with a deregulation of lipid metabolism, leading to the accumulation of triglycerides (steatosis) in the liver (53). Here we found that the marked liver steatosis observed in ED-exposed animals was linked to the deregulation of several genes controlling lipid metabolism. Indeed, we found a marked under-transcription of *sulfotransferase 2b1* (*sult2b1*) (0.21 for BaP and 0.35-fold for TCS), an enzyme known to protect the liver from steatosis and to inhibit lipogenesis (54). Moreover, BaP-exposed animals presented a marked deregulation of the *patatin-like phospholipase domain containing 3* (*pnpla3*, 0.26-fold) gene whose inhibition has been associated with lipid accumulation in the liver (55). In TCS-exposed animals, several genes associated with liver triglyceride or cholesterol accumulation were found to be overtranscribed, including the *7-dehydrocholesterol reductase* (*dhcr7*, 2.75-fold) and the *Kruppel-like factor 2* (*klf2*, 2.52-fold) (33, 56).

As described above, physiological observations indicated a gradation between liver manifestations of IR in ED-exposed animals. Liver symptoms varied from NAFLD for TCS-exposed animals to a progression to NASH in BaP-exposed *Xenopus* (Fig1). Transcriptomic data confirmed these phenotypes with a higher number of genes highlighting the severity of liver dysfunction for BaP exposure. Indeed, we found a marked under-transcription of several genes involved in lipid metabolism (*acss2.2*, 0.24-fold; *elovl2*, 0.35-fold; *hmgcs1*, 0.31-fold; *mgat2*, 0.34-fold) for which a deregulation has been associated with the progression from NAFLD to NASH (57). NASH is also associated with inflammatory processes (43). Here we found that the leukocyte infiltrates observed in BaP-exposed animals were associated with the deregulation of key genes involved in inflammation including *cd3e* (3.15-fold), *cd40* (3.34-fold), *fas* (2.11-fold), *gadd45g* (2.15-fold), *susd1* (3.15-fold), *vasp* (0.48-fold), *vegfc* (2.75-fold).

BaP-induced metabolic syndrome and glucose intolerance are not reversible

In order to test the reversibility of the symptoms observed we performed a one-year depuration of the exposed animals. Interestingly, whereas the glucose intolerance phenotype appeared reversible in TCS-exposed *Xenopus*, individuals exposed to BaP remained glucose intolerant after one year of depuration in clean water (Fig. 3a). However, whichever ED was considered, the depurated animals still displayed a marked increase in their hepatosomatic index correlated with marked hepatic steatosis (Fig. 3b-c). These hepatic manifestations were accompanied by a marked insulin secretory defect regardless of the ED exposure considered (Fig.3d). Since only the BaP-exposed animals remained glucose intolerant, our results suggest that the marked liver damage induced by this ED is not reversible.

ED-induced metabolism impairments are associated with decreased fitness and multi-generational effects.

Our data reveal that ED at environmental concentrations induce a marked metabolic impairment in female *Xenopus,* on which the resources found in the eggs are entirely dependent (58). In order to test the consequences of parental exposure on their progeny, these females were mated with exposed males. Out of the five matings we performed for each exposure condition, only two were successful in TCS-exposed animals. Indeed, despite their appropriate sexual maturity, three out of five TCS-exposed females did not accept the male, suggesting that TCS impairs sexual behavior in amphibians, as has been previously described in fish (59).

Like their BaP-exposed genitor, the progeny not directly exposed to ED showed a significant time delay to metamorphosis (35 days more to reach 90% frog metamorphosis in the population (Fig. 4a) demonstrating the multigenerational impact of ED. Moreover, regardless of the ED considered, successful mating produced F1 individuals of smaller size and weight (Fig 4 a-b)

demonstrating a multigenerational aggravation of the phenotype observed in their genitors. These results may have a major impact on amphibian population decline. Indeed, delayed metamorphosis, along with decreased size at metamorphosis reduces adult recruitment and the likelihood of reproduction in amphibians (60). Smaller size at metamorphosis limits food availability for newly-metamorphosed frogs because of gape limitation and increases their vulnerability to predators which are also gape-limited (61). In addition, decreased size at metamorphosis combined with subsequent decreased post-metamorphic growth decreases the amphibians' chances of surviving overwintering. This negative effect is especially true for females, for which size is directly proportional to fecundity (62). Here we found that F1 females from BaP-exposed genitors showed a significant time delay to achieving sexual maturity (141 days more to reach 90% female mature in the population (Fig. 4 c). In order to evaluate the reproductive success of F1 progeny and to study the fitness of their exposed genitors, five matings were performed with F1 animals from control and BaP-exposed parents, and only one for TCS (corresponding to the only two adult *Xenopus* surviving from F0 matings under this condition). Interestingly, regardless of the ED considered, a disturbance in mating behavior was observed, characterized by a delayed time for amplexus formation. At three hours post stimulation; only two amplexus were successful for F1 from BaP parental exposure and that from TCS parental exposure was not successful (Fig. 4e). F1 mates performed for each parental exposure resulted in a highly variable number of hatched eggs. However, a strong tendency revealed a dramatic decrease in the number of eggs hatched by F1 individual from BaP and TCS-exposed parents (Fig. 4f) suggesting a decrease fitness induced by ED exposure.

Much emphasis has been placed on implicating ED in amphibian population decline. As suggested by epidemiological studies in humans, we found that ED can induce severe metabolic disorders in amphibians at concentrations in the range of those considered safe for higher vertebrates. Moreover, parental exposure to ED can alter the development and the reproduction

of their progeny, which could result in decreased fitness. Taken as a whole, the findings from this study constitute a starting point for considering ED as a contributing cause of amphibian population decline through their disruption of energetic metabolism, and provide new insights into the transgenerational effects of ED, not only in amphibians, but also in higher vertebrates including humans

Methods

Animals

Pre-metamorphic *Xenopus tropicalis* aged seven days were purchased from the "*Xenopus* national husbandry" (CRB "Xenopes"), University of Rennes 1 (http://xenopus.univ-rennes1.fr/). They were allowed to acclimatize for one week at 25°C with a photoperiod of 12:12 hours in Marc's Modified Ringer's (MMR) 0.1X medium (pH 7.4, NaCl = 10 mM, KCl = 2×10^{-1} mM, $MgSO_4$ = 10^{-1} mM, $CaCl_2$ = 2×10^{-1} mM, HEPES = 5×10^{-1} mM) prior to starting the experiments. The frogs were fed daily *ad libitum* with finely ground pellets of trout food (Aquatic 3, Special Diets Services) and the grinding level was adjusted to the size of their jaw throughout their growth. The density of young tadpoles aged two weeks was 50 individuals per 2 L of medium, corresponding to 2 tanks per exposure condition, conditions described below. To satisfy the volume needed over the growth period, frogs were moved to larger tanks prior to the metamorphosis stage (2 tanks of 30 individuals aged 30 days per 4 L of medium, for each condition). At the end of metamorphosis *Xenopus* were dispatched into 4 tanks (10 individuals aged 150 days per 4 L of medium, for each condition). All experiments were performed in an animal house accredited by the French Ministry of Animal Welfare (i.e. Rovaltain research

company, n° A 26 004 1401) and in accordance to the recommendations of the ethics committee ComEth Grenoble - C2EA - 12 (animal welfare agreement n° 02545.03).

Xenopus exposure to benzo[*a*]pyrene (B*a*P) and triclosan (TCS)

Xenopus were exposed collectively at 25°C in tanks (150 tadpoles per condition). The medium was partially renewed every day (1/4 of the total volume) and completely renewed weekly with a solution of MMR containing either B*a*P (97% purity, Sigma-Aldrich, St-Louis, MO, USA) or TCS (97% purity, Sigma-Aldrich) at an initial concentration of 200 $ng.L^{-1}$. The control frogs were exposed to Dimethyl sulfoxide (DMSO, vehicle) at 4/1000 (v:v) concentration. Concentrations of pollutants in the media over time were controlled by GC-MS / MS. For this purpose, freshly prepared and contaminated media were placed in the same tanks and with the same light, temperature and *Xenopus* density conditions for populations exposed during the experiment. The results (not shown) reveal that 85% of B*a*P and 87% of TCS were absorbed within 24 hours and that the periodicity of the medium change was equivalent to a weekly average concentration of 50 $ng.L^{-1}$. These concentrations were chosen to match the B*a*P or TCS concentrations usually found in polluted waters (34, 35) and are in the range of maximal safe drinking water concentrations for BaP (36, 37), no data for TCS available yet.

After 12 months of exposure, 4 females for each exposure condition were used to perform a glucose tolerance test and 8 others (divided in two pools of four to ensure sufficient material for performing all experiments) were rapidly sacrificed with a blow to the head and immediately dissected to sample the liver, the pancreas and the muscles. Blood was collected by means of an intra-cardiac puncture. For each exposure condition three females were transferred into clean medium and maintained for 12 months to mimic a depuration period. The organ sampling procedure was carried out as previously described.

Hepatosomatic index.

Each *Xenopus* and their liver were weighed to the nearest 0.1 mg and the hepatosomatic index (HSI) was calculated as follows:

$$HSI = (\text{liver weight [g]}) \times (\text{total body weight [g]})^{-1} \times 100$$

Histological observations

After dissection, the liver (same lobe/frog) and the pancreas were embedded in Tissue OCT (Labonord - VWR, Templemars, France), immediately flash frozen in liquid nitrogen, and conserved at -80°C. Transverse sections (7 µm) were produced using a cryostat (CM3050 S, Leica, Nussloch, Germany) with the temperature of the cryochamber and specimen set at -25°C. Frozen sections were mounted on Super-Frost plus microscope slides (Labonord).

The frozen sections of the liver were stained with Oil Red O (ORO) to assess total lipid hepatic content as previously described (33).

Hepatic glycogen content was estimated using Periodic Acid Schiff (PAS) staining. The slides were briefly rinsed in water and incubated with 0.5% periodic acid for 10 min before staining with Schiff reagent for 15 min and hematoxylin for 1 min. The sections were dehydrated by 1 min incubation in 70% ethanol, followed by 1 min incubation in 95% ethanol, followed by 1 min incubation in toluene. PAS scoring was performed by two people independently. PAS staining score (0 to 4) was assigned depending on the percentage of glycogen in cells. A score of 0 corresponds to one cell without glycogen and a score of 4 corresponds to one cell filled with glycogen.

Frozen pancreas sections were fixed for 10 min in 4% formaldehyde and washed in phosphate buffered saline (PBS) containing 0.5% bovine serum albumin (BSA). A saturation step was

performed for 30 min in PBS containing 5% BSA. The sections were then incubated overnight at 4°C with guinea pig anti-human insulin serum (Y370; Yanaihara Institute, Fujinomiya, Japan) diluted 1:500 in PBS-BSA 0.5%. The sections were then washed again in PBS-BSA 0.5% and incubated with goat anti-guinea pig IgG (H+L) FITC-conjugated (SouthernBiotech) diluted 1:200 in PBS-BSA 0.5%, for 30 min at room temperature, in the dark. We used the Converter AP (Roche) on the frozen sections according to the manufacturer's instructions to convert the fluorescence signal into a colorimetric signal. Revelation was performed using Fast Red (Sigma-Aldrich, France) as substrate for 15 min. After labelling, the frozen sections were counterstained with Mayer's Haemalun (Merck, Germany) and mounted with aqueous mounting medium (aquatex®,Merck, Germany). Each slide (one per animal) was photographed under a Nikon Eclipse E600 microscope using an Olympus DP70 digital camera. Two to five pictures were taken, corresponding to the five hot spots of insulin labelling by section. Each picture was imported into the GNU Image Manipulation Program (GIMP v2.8.6) and the area of each labelling acini found in the pictures was quantified with the histogram dialog. Because the insulin appeared magenta on the pictures, the labelling intensity was estimated by the inverse of the green channel level, again using the histogram dialog. For each slide, this intensity was quantified as previously described (33) and used to standardize acini intensity. Insulin production was obtained as a multiplication of the acinus area by the standardized labelling intensity for each acinus.

Hepatic mitochondrial respiration

The mitochondria were prepared as described in Garait et al. (63) (isolation medium: pH 7.4, 250 mM sucrose, 20 mM Tris, 1 mM EGTA). Mitochondrial protein concentration was determined with a Pierce modified Lowry protein assay, according to the manufacturer's instructions (ThermoFisher Scientific). The mitochondrial oxygen consumption rate was measured

polarographically with a Clark oxygen electrode, in a closed and stirred glass cell. The respiration medium (pH 7.2, 125 mM KCl, 20 mM Tris, 5 mM Pi, 1 mM EGTA) was supplemented with 5 mM glutamate, 2.5 mM malate and 5 mM succinate for measuring complex I and complex II–mediated mitochondrial respiration (State 2). States 3 respiration was measured after the addition of 500 mM adenosine diphosphate (ADP) and the respiratory control index (RCI) was defined as the ratio state 3/state 2.

Liver proteasome activity

Peptidase activity of the proteasome was assayed using a fluorogenic peptide, succinyl-Leu-Leu-Val-Tyr-7-Amido-4-Methylcoumarin (LLVY-AMC) Sigma-Aldrich (Saint Quentin Falavier, France) as previously described (64).

Liver aconitase activity

Mitochondria were suspended in 25 mM phosphate buffer pH 7.25 supplemented with 0.05% Triton X-100 and aconitase activity was assayed spectrophotometrically at 340 nm, as previously described (39).

Liver citrate synthase activity

Citrate synthase activity was measured as the rate of appearance of thionitrobenzoic acid followed by the increase of absorbance at 412 nm during 3 min in the presence of 10 µg of isolated mitochondria proteins, 100 mM Tris–HCl pH8.0, 0.1%Triton X100, 300 mM acetylCoA, 100µM DTNB, and 500 µM oxaloacetate.

Muscle glycogen content

40 mg of muscle were lysed in 40% KOH at 100°C during 30 min before cooling and glycogen precipitation with 100% ethanol during one night at – 20°C. After centrifugation at 10,000 x g for 15 min at 4°C, the glycogen pellet was hydrolyzed in glucose by incubation in 2N HCL at 100°C during 3h. After neutralization with 2N NaOH, the concentration of glucose was measured with the GAGO-20 kit (Sigma Aldrich, France) following the manufacturer's instructions.

Glucose tolerance test

Blood glucose was measured by digital sampling, 0, 1, 2, and 4 h after glucose injection in the dorsal lymph sac (1 $mg.g^{-1}$ fresh mass) using a handheld plasma calibrated glucometer (Accu-Chek performa, Roche Diagnostics, Meylan, France). For statistical comparison, areas under curve after glucose challenge were used.

Alanine aminotransferase activity in the serum

Serum was obtained from fresh blood centrifugation (3,000 × g for 10 min at 4 °C) and stored at -80°C. Alanine aminotransferase (ALAT) activity was measured using 3 mL of pure *Xenopus* serum, according to the manufacturer's instructions (Alanine Aminotransferase Activity Assay Kit, Sigma-Aldrich).

Plasma Triglyceride measurements

Plasma total triglyceride concentrations were determined using a triglycerides GPO-PED kit (Sobioda, France).

Statistics

For F0 individual data are expressed as the mean ± SEM. Each value was derived from 4 individual experiments for frogs immediately sacrificed after 12 months' exposure and from 3 individual experiments for frogs sacrificed after 12 months of depuration post-exposure. Since the nature of the distribution of the results was unknown (Gaussian or not) for 4 or 3 replicates, the comparison of each treatment (either B*a*P or TCS) with a single control, was performed using a Wilcoxon test.

The distributions of F0 and F1 individual development times were compared between control populations and each parental ED-exposed population separately with a Kaplan-Meyer test to evaluate global curve differences.

The distribution of F0 and F1 female maturity time between control populations and each parental ED-exposed population was determined separately with a Kaplan-Meyer test to evaluate global curve differences.

For the comparison of the size and weight of F1 individuals, since the nature of the distribution of the results was not Gaussian for TCS parental exposure, the comparison of each parental treatment (either B*a*P or TCS) with a single control, was performed using a Wilcoxon test.

Liver RNA extraction and sequencing

For each biological replicate, total RNA was extracted from 15 mg liver using the RNAqueous®-4PCR Kit (Ambion, USA) according to manufacturer's instructions. Total RNA quality and quantity were controlled on an Agilent 2100 Bioanalyzer (Agilent, USA). RNA-seq libraries were prepared using the TruSeq Stranded mRNA sample Prep kit (Illumina) and sequenced on an Illumina GAIIx sequencer as 75 bp reads by Hybrigenics-Helixio (Clermont-Ferrand, France).

Mapping reads on the *Xenopus* genome

Sequenced reads were assigned to each sample (unplexing) and adaptors were removed. The quality of the reads for each sample was checked using FastQC. The reads were then filtered based on their length, pairing and quality using Trimmomatic (v0.32.1) (65). Cleaned reads were mapped to the *Xenopus* genome (JGI4.2 assembly) with Ensembl annotations (release 79) using Bowtie-0.12.7 / TopHat 2 (v0.6) software (66) (http://tophat.cbcb.umd.edu) (with a maximum intron size of 250,000 bp to discover novel junctions between exons).

Gene expression quantification and differential analysis

The Cufflinks (v0.0.7) tool was applied to TopHat alignments to enumerate for each library the number of short reads overlapping the Ensembl annotated genes (67). The Cuffmerge (v0.0.6) script implanted in Cufflinks was used to merge multiple assemblies from each sample. Gene transcription levels were computed from alignments carried out using TopHat 2 and compared statistically using the Cuffdiff (v0.0.7) tool implemented in a Galaxy pipeline (http://galaxyproject.org). Genes were considered differentially transcribed when the transcription ratio TR (B*a*P or TCS treated/control) was > 1.8 in either direction with an adjusted *p*-value lower than 0.05 after multiple testing correction.

Functional annotation enrichment

Differentially expressed genes were subjected to annotation enrichment analysis and Kyoto Encyclopedia of Genes and Genomes (KEGG) pathway mapping using the online functional annotation tool DAVID (Database for Annotation, Visualisation and Integrated Discovery, http://david.abcc.ncifcrf.gov/) (68) with all the genes detected in our experiment as background (9,310 genes). *Xenopus* gene identifiers were transformed into their human orthologs to improve the richness of the output as previously described (33). Significance was calculated using a modified Fisher 's Exact test ($p < 0.05$). Heat maps of expression profiles for genes sharing enriched annotation pathways or other genes associated with these pathways were produced using TM4 Multi experiment Viewer (MeV) software (69).

Xenopus mating and progeny development

At the end of the exposure period, five F0 females and ten F0 males per condition were naturally mated. Mating behavior was induced by two injections of human chorionic gonadotropin (hCG) in the dorsal lymph sac of each *Xenopus* as previously described (70). After hatching, tadpoles were bred has described above. F1 development was characterized by the time from hatching to metamorphosis together with the snout-vent length and the weight at metamorphosis. At adult stage, F1 animals were mated as described before.

Data access

RNA-seq sequence data have been deposited at EMBL-EBI (http://www.ebi.ac.uk/ena) under the accession number PRJEB18463.

Acknowledgements

This work was funded by the IRS-IDEX Grant of the ComUE Université Grenoble-Alpes. Christophe Regnault was funded by Ministry of Higher Education and Research. Marie Usal was funded by the Région Auvergne-Rhône-Alpes.

Author Contributions:

CR and MU prepared the samples, performed mRNAseq and histological experiments, analyzed data, performed statistical analyses and helped to draft the manuscript; SV performed histological manipulations; KC and CB performed mitochondrial experimentations; ALB performed proteasome, aconitase and citrate synthase experiments; DL, AS and BC were in charge of animal rearing and exposure; MC and CLM performed plasma triglyceride measurements; MR designed the study, participated in sample preparation, participated in data analyses and participated in writing the manuscript; SR conceived and coordinated the study, participated in sample preparation, analyzed data and wrote the manuscript. All authors read and approved the final manuscript.

References

1. Lips KR, Diffendorfer J, Mendelson JR, Sears MW (2008) Riding the wave: reconciling the roles of disease and climate change in amphibian declines. *PLoS biology* 6(3):e72.
2. Roelants K*, et al.* (2007) Global patterns of diversification in the history of modern amphibians. *Proceedings of the National Academy of Sciences of the United States of America* 104(3):887-892.
3. Hayes TB, Falso P, Gallipeau S, Stice M (2010) The cause of global amphibian declines: a developmental endocrinologist's perspective. *Journal of Experimental Biology* 213(6):921-933.
4. Carey C, Cohen N, Rollins-Smith L (1999) Amphibian declines: an immunological perspective. *Developmental and comparative immunology* 23(6):459-472.
5. Kiesecker JM (2002) Synergism between trematode infection and pesticide exposure: a link to amphibian limb deformities in nature? *Proceedings of the National Academy of Sciences of the United States of America* 99(15):9900-9904.
6. Fedorenkova A*, et al.* (2012) Ranking ecological risks of multiple chemical stressors on amphibians. *Environmental toxicology and chemistry* 31(6):1416-1421.
7. Kaplan M (2009) Amphibians rarely give earliest warning of pollution. *J. Exp. Biol.* Available from: http://www.nature.com/news/2009/091029/full/news.2009.1048.html.
8. Helbing CC (2012) The metamorphosis of amphibian toxicogenomics. *Frontiers in genetics* 3:37.
9. Langlois VS*, et al.* (2010) Fadrozole and finasteride exposures modulate sex steroid- and thyroid hormone-related gene expression in Silurana (Xenopus) tropicalis early larval development. *General and comparative endocrinology* 166(2):417-427.
10. Crump D, Werry K, Veldhoen N, Van Aggelen G, Helbing CC (2002) Exposure to the herbicide acetochlor alters thyroid hormone-dependent gene expression and metamorphosis in Xenopus Laevis. *Environmental health perspectives* 110(12):1199-1205.

11. Opitz R*, et al.* (2005) Description and initial evaluation of a Xenopus metamorphosis assay for detection of thyroid system-disrupting activities of environmental compounds. *Environmental toxicology and chemistry* 24(3):653-664.
12. Hammond SA, Veldhoen N, Helbing CC (2015) Influence of temperature on thyroid hormone signaling and endocrine disruptor action in Rana (Lithobates) catesbeiana tadpoles. *General and comparative endocrinology* 219:6-15.
13. Hayes TB*, et al.* (2010) Atrazine induces complete feminization and chemical castration in male African clawed frogs (Xenopus laevis). *Proceedings of the National Academy of Sciences of the United States of America* 107(10):4612-4617.
14. Hayes T*, et al.* (2002) Herbicides: feminization of male frogs in the wild. *Nature* 419(6910):895-896.
15. Duarte-Guterman P, Navarro-Martin L, Trudeau VL (2014) Mechanisms of crosstalk between endocrine systems: regulation of sex steroid hormone synthesis and action by thyroid hormones. *General and comparative endocrinology* 203:69-85.
16. Hayes TB*, et al.* (2011) Demasculinization and feminization of male gonads by atrazine: consistent effects across vertebrate classes. *The Journal of steroid biochemistry and molecular biology* 127(1-2):64-73.
17. Fan W*, et al.* (2007) Atrazine-induced aromatase expression is SF-1 dependent: implications for endocrine disruption in wildlife and reproductive cancers in humans. *Environmental health perspectives* 115(5):720-727.
18. Fan W*, et al.* (2007) Herbicide atrazine activates SF-1 by direct affinity and concomitant co-activators recruitments to induce aromatase expression via promoter II. *Biochemical and biophysical research communications* 355(4):1012-1018.
19. Hayes TB*, et al.* (2006) Characterization of atrazine-induced gonadal malformations in African clawed frogs (Xenopus laevis) and comparisons with effects of an androgen antagonist (cyproterone acetate) and exogenous estrogen (17beta-estradiol): Support for

the demasculinization/feminization hypothesis. *Environmental health perspectives* 114 Suppl 1:134-141.

20. Hayes TB*, et al.* (2002) Hermaphroditic, demasculinized frogs after exposure to the herbicide atrazine at low ecologically relevant doses. *Proceedings of the National Academy of Sciences of the United States of America* 99(8):5476-5480.
21. Urbatzka R, Bottero S, Mandich A, Lutz I, Kloas W (2007) Endocrine disrupters with (anti)estrogenic and (anti)androgenic modes of action affecting reproductive biology of Xenopus laevis: I. Effects on sex steroid levels and biomarker expression. *Comparative biochemistry and physiology. Toxicology & pharmacology : CBP* 144(4):310-318.
22. Cevasco A*, et al.* (2008) Endocrine disrupting chemicals (EDC) with (anti)estrogenic and (anti)androgenic modes of action affecting reproductive biology of Xenopus laevis: II. Effects on gonad histomorphology. *Comparative biochemistry and physiology. Toxicology & pharmacology : CBP* 147(2):241-251.
23. Orton F,Tyler CR (2015) Do hormone-modulating chemicals impact on reproduction and development of wild amphibians? *Biological reviews of the Cambridge Philosophical Society* 90(4):1100-1117.
24. Safholm M, Ribbenstedt A, Fick J, Berg C (2014) Risks of hormonally active pharmaceuticals to amphibians: a growing concern regarding progestagens. *Philosophical transactions of the Royal Society of London. Series B, Biological sciences* 369(1656).
25. Casals-Casas C,Desvergne B (2011) Endocrine disruptors: from endocrine to metabolic disruption. *Annual review of physiology* 73:135-162.
26. Chevalier N,Fenichel P (2015) Endocrine disruptors: new players in the pathophysiology of type 2 diabetes? *Diabetes & metabolism* 41(2):107-115.
27. Chevalier N,Fenichel P (2015) Bisphenol A: Targeting metabolic tissues. *Reviews in endocrine & metabolic disorders* 16(4):299-309.

28. Chevalier N,Fenichel P (2016) [Endocrine disruptors: A missing link in the pandemy of type 2 diabetes and obesity?]. *Presse medicale* 45(1):88-97.
29. Jiang Y*, et al.* (2014) Mitochondrial dysfunction in early life resulted from perinatal bisphenol A exposure contributes to hepatic steatosis in rat offspring. *Toxicology letters* 228(2):85-92.
30. Alonso-Magdalena P*, et al.* (2010) Bisphenol A exposure during pregnancy disrupts glucose homeostasis in mothers and adult male offspring. *Environmental health perspectives* 118(9):1243-1250.
31. Susiarjo M*, et al.* (2015) Bisphenol a exposure disrupts metabolic health across multiple generations in the mouse. *Endocrinology* 156(6):2049-2058.
32. Regnault C*, et al.* (2016) Metabolic and immune impairments induced by the endocrine disruptors benzo[a]pyrene and triclosan in Xenopus tropicalis. *Chemosphere* 155:519-527.
33. Regnault C*, et al.* (2014) Impaired liver function in Xenopus tropicalis exposed to benzo[a]pyrene: transcriptomic and metabolic evidence. *BMC genomics* 15:666.
34. Dortch MS, Zakikhani M, Kim SC, Steevens JA (2008) Modeling water and sediment contamination of Lake Pontchartrain following pump-out of Hurricane Katrina floodwater. *Journal of environmental management* 87(3):429-442.
35. Perez AL*, et al.* (2013) Triclosan occurrence in freshwater systems in the United States (1999-2012): a meta-analysis. *Environmental toxicology and chemistry* 32(7):1479-1487.
36. Canada H (2016) Guidelines for Canadian Drinking Water Quality: Guideline Technical Document — Benzo[a]pyrene. Water and Air Quality Bureau, Healthy Environments and Consumer Safety Branch, Health Canada, Ottawa, Ontario.
37. WHO (2003) Polynuclear aromatic hydrocarbons in Drinking-water. Background document for development of WHO. in *Guidelines for drinking-water quality* (World Health Organization, Geneva).

38. Koliaki C*, et al.* (2015) Adaptation of hepatic mitochondrial function in humans with non-alcoholic fatty liver is lost in steatohepatitis. *Cell metabolism* 21(5):739-746.

39. Bulteau AL, Ikeda-Saito M, Szweda LI (2003) Redox-dependent modulation of aconitase activity in intact mitochondria. *Biochemistry* 42(50):14846-14855.

40. Yamaguchi K*, et al.* (2007) Inhibiting triglyceride synthesis improves hepatic steatosis but exacerbates liver damage and fibrosis in obese mice with nonalcoholic steatohepatitis. *Hepatology* 45(6):1366-1374.

41. Otoda T*, et al.* (2013) Proteasome dysfunction mediates obesity-induced endoplasmic reticulum stress and insulin resistance in the liver. *Diabetes* 62(3):811-824.

42. Kasuga M (2006) Insulin resistance and pancreatic beta cell failure. *The Journal of clinical investigation* 116(7):1756-1760.

43. Takahashi Y,Fukusato T (2014) Histopathology of nonalcoholic fatty liver disease/nonalcoholic steatohepatitis. *World journal of gastroenterology* 20(42):15539-15548.

44. Michurina SV*, et al.* (2016) Linagliptin alleviates fatty liver disease in diabetic db/db mice. *World journal of diabetes* 7(19):534-546.

45. Petersen KF*, et al.* (2007) The role of skeletal muscle insulin resistance in the pathogenesis of the metabolic syndrome. *Proceedings of the National Academy of Sciences of the United States of America* 104(31):12587-12594.

46. Satyarengga M, Zubatov Y, Frances S, Narayanswami G, Galindo RJ (2017) Glycogenic Hepatopathy: A Complication of Uncontrolled Diabetes. *AACE clinical case reports* 3(3):e255-e259.

47. Pagliassotti MJ, Kim PY, Estrada AL, Stewart CM, Gentile CL (2016) Endoplasmic reticulum stress in obesity and obesity-related disorders: An expanded view. *Metabolism: clinical and experimental* 65(9):1238-1246.

48. Bensellam M*, et al.* (2016) Hypoxia reduces ER-to-Golgi protein trafficking and increases cell death by inhibiting the adaptive unfolded protein response in mouse beta cells. *Diabetologia* 59(7):1492-1502.

49. Bechmann LP*, et al.* (2012) The interaction of hepatic lipid and glucose metabolism in liver diseases. *Journal of hepatology* 56(4):952-964.

50. Burri L, Thoresen GH, Berge RK (2010) The Role of PPARalpha Activation in Liver and Muscle. *PPAR research* 2010.

51. Brismar K, Fernqvist-Forbes E, Wahren J, Hall K (1994) Effect of insulin on the hepatic production of insulin-like growth factor-binding protein-1 (IGFBP-1), IGFBP-3, and IGF-I in insulin-dependent diabetes. *The Journal of clinical endocrinology and metabolism* 79(3):872-878.

52. Pei L*, et al.* (2006) NR4A orphan nuclear receptors are transcriptional regulators of hepatic glucose metabolism. *Nature medicine* 12(9):1048-1055.

53. Naik A, Kosir R, Rozman D (2013) Genomic aspects of NAFLD pathogenesis. *Genomics* 102(2):84-95.

54. Musso G, Gambino R, Cassader M (2013) Cholesterol metabolism and the pathogenesis of non-alcoholic steatohepatitis. *Progress in lipid research* 52(1):175-191.

55. Mondul A*, et al.* (2015) PNPLA3 I148M Variant Influences Circulating Retinol in Adults with Nonalcoholic Fatty Liver Disease or Obesity. *The Journal of nutrition* 145(8):1687-1691.

56. Chen JL, Lu XJ, Zou KL, Ye K (2014) Kruppel-like factor 2 promotes liver steatosis through upregulation of CD36. *Journal of lipid research* 55(1):32-40.

57. Nagaya T*, et al.* (2010) Down-regulation of SREBP-1c is associated with the development of burned-out NASH. *Journal of hepatology* 53(4):724-731.

58. Di Croce L, Bruscalupi G, Trentalance A (1997) Independent responsiveness of frog liver low-density lipoprotein receptor and HMGCoA reductase to estrogen treatment. *Pflugers Archiv : European journal of physiology* 435(1):107-111.

59. Schultz MM, Bartell SE, Schoenfuss HL (2012) Effects of triclosan and triclocarban, two ubiquitous environmental contaminants, on anatomy, physiology, and behavior of the fathead minnow (Pimephales promelas). *Archives of environmental contamination and toxicology* 63(1):114-124.

60. Smith D (1987) Adult recruitment in chorus frogs: effects of size and date at metamorphosis. *Ecology* 68:344-350.

61. De Vito J, Chivers D, Kiesecker J, Belden L, Blaustein A (1999) Effects of snake predation on aggregation and metamorphosis of Pacific treefrog (Hyla regilla) larvae. *J Herpetol* 33 504–507.

62. Hayes TB*, et al.* (2006) Pesticide mixtures, endocrine disruption, and amphibian declines: are we underestimating the impact? *Environmental health perspectives* 114 Suppl 1:40-50.

63. Garait B*, et al.* (2005) Fat intake reverses the beneficial effects of low caloric intake on skeletal muscle mitochondrial H(2)O(2) production. *Free radical biology & medicine* 39(9):1249-1261.

64. Bulteau AL, Szweda LI, Friguet B (2002) Age-dependent declines in proteasome activity in the heart. *Archives of biochemistry and biophysics* 397(2):298-304.

65. Bolger AM, Lohse M, Usadel B (2014) Trimmomatic: a flexible trimmer for Illumina sequence data. *Bioinformatics* 30(15):2114-2120.

66. Trapnell C, Pachter L, Salzberg SL (2009) TopHat: discovering splice junctions with RNA-Seq. *Bioinformatics* 25(9):1105-1111.

67. Trapnell C*, et al.* (2012) Differential gene and transcript expression analysis of RNA-seq experiments with TopHat and Cufflinks. *Nature protocols* 7(3):562-578.

68. Huang da W, Sherman BT, Lempicki RA (2009) Bioinformatics enrichment tools: paths toward the comprehensive functional analysis of large gene lists. *Nucleic acids research* 37(1):1-13.

69. Saeed AI*, et al.* (2003) TM4: a free, open-source system for microarray data management and analysis. *BioTechniques* 34(2):374-378.

70. Showell C,Conlon FL (2009) Natural mating and tadpole husbandry in the western clawed frog Xenopus tropicalis. *Cold Spring Harbor protocols* 2009(9):pdb prot5292.

Figure legends

Fig. 1: Endocrine disruptor exposure leads to metabolic impairments in *Xenopus*. a, glucose tolerance test. **b**, relative Hepatosomatic indexes of control and exposed animals. **c**, oil Red O staining for total lipid content measured in the livers of control and exposed animals. Lipid content is indicated by red staining. Scale bars = 25 µm. Relative Oil Red O area in the livers of control and exposed animals are represented by the histograms. **d**, relative blood triglycerides concentrations. **e**, relative mitochondrial State 2 respiration rate in liver of control and exposed animals. **f**, relative mitochondrial respiratory control indexes in liver of control and exposed animals. **g**, relative aconitase activity in control and exposed animals. **h**, relative citrate synthase activity in control and exposed animals. **i**, relative ALAT activity in control and exposed animals. **j**, H&E stain of liver sections of control animals. Scale bars= 70 µm. **k**, H&E stain of liver sections of BaP-exposed animals. Arrow indicates an area of ballooning hepatocytes. Scale bars= 70 µm. **l**, H&E stain of liver sections of TCS-exposed animals. Scale bars= 70 µm. **m**, Gomori's Trichrom stain of sections of control animals. Scale bars= 70 µm**. n,** Gomori's Trichrom stain of liver sections of BaP-exposed animals. Arrow indicates necrotic area with leukocyte infiltrates. Scale bars= 70 µm. **o**, Gomori's Trichrom stain of liver sections of TCS-exposed animals. Arrow indicates dilated blood vessel. Scale bars= 70 µm. **p**, relative proteasome activity in the livers of control and exposed animals. **q**, insulin immunostaining of the pancreas of control and exposed animals. Insulin content is indicated by red staining. Scale bars= 25 µm. Relative insulin quantity estimated by area x intensity of islet stained for Insulin in the pancreas of control and exposed animals is represented by the histograms. **r**, relative glycogen content in the muscles of control and exposed animals. The statistical analysis was performed using Wilcoxon test. The asterisks indicate a significant difference from the control: *, $p < 0.05$, n=4 per exposure group. **s**, relative glycogen content in the livers of control and exposed animals. The

statistical analysis was performed using the Wilcoxon's test. The asterisks indicate a significant difference from the control: *, $p < 0.05$, n=4 per exposure group.

Fig. 2: Liver transcriptome following endocrine disruptor exposure indicates a marked metabolic impairment typical of IR syndrome. a, the genes showing a significant differential transcription from control in at least one condition were used for annotation enrichment using the DAVID (Database for Annotation, Visualisation and Integrated Discovery) functional annotation tool (modified Fisher's Exact test with $p < 0.05$). Histograms indicate the level of enrichment of the pathways found to be significantly enriched in BaP- or TCS-exposed animals. **b-d**, transcription of genes involved in the different pathways. The color scale indicates transcription ratios relative to the controls. The black boxes indicate the pathway highlighted by the gene found to be differentially transcribed compared to the control. Pathways have been grouped according to their parent root in KEGG description. **e**, transcription of genes involved in the immune system or specifically found to be involved in NAFLD/NASH syndrome in the literature. The black boxes indicate the pathway highlighted by the gene found to be differentially transcribed compared to the control. NS indicates that the gene considered was not found to be differentially transcribed compared to the control in the considered exposure. n=4 per exposure group.

Fig. 3: Persistence of metabolic impairments in *Xenopus* after one year of depuration. a, glucose tolerance test. **b,** relative Hepatosomatic indexes of control and exposed animals. **c,** oil Red O staining for total lipid content measured in the livers of control and exposed animals. Lipid content is indicated by red staining. Scale bars = 25 µm. Relative Oil Red O area in the livers of control and exposed animals are represented by the histograms. **d**, insulin immunostaining of

the pancreas of control and exposed animals. Insulin content is indicated by red staining. Scale bars= 25 µm. Relative insulin quantity estimated by area x intensity of islet stained for Insulin in the pancreas of control and exposed animals is represented by the histograms. The statistical analysis was performed using the Wilcoxon test. The asterisks indicate a significant difference from the control: *, $p < 0.05$, n=3 per exposure group.

Fig. 4: Parental exposure to endocrine disruptors leads to delayed metamorphosis time and reduced size and weight of progeny. a, development curves of F1 individuals from hatching to metamorphosis. The distributions of F1 individual development times were compared between control populations and each parental ED-exposed population separately with a Kaplan-Meyer test to evaluate global curve difference. The asterisks indicate a significant difference from the control: *, $p < 0.05$ (n= 716, 1020 and 72 for control, BaP and TCS parental exposure). **b,** snout-vent length of F1 individual at metamorphosis from each parental exposure. **c,** weight of F1 individual at metamorphosis from each parental exposure. The statistical analysis was performed using the Wilcoxon test. The asterisks indicate a significant difference from the control: *, $p < 0.05$ (n= 46, 63 and 10 for control, BaP and TCS parental exposure respectively). **d,** development curves of F1 juvenile female from hatching to sexual maturity. The distributions of F1 individual development times were compared between control populations and each parental ED-exposed population separately with a Kaplan-Meyer test to evaluate global curve difference The asterisks indicate a significant difference from the control: *, $p < 0.05$ (n= 10, 28 and 1 for control, BaP and TCS parental exposure). **e,** percentage of successful amplexus at 3 hrs post-stimulation of F1 animals (n= 5, 5 and 1 for control, BaP and TCS parental exposure). **f,** number of hatching eggs per F1 female from each successful amplexus (n= 5, 5 and 1 for control, BaP and TCS parental exposure).

Supplementary figure legends

Fig. S1: Exposure to endocrine disruptors leads to delayed metamorphosis time

a, development curves of F0 individuals from hatching to metamorphosis. The distributions of F0 individual development times were compared between control populations and each parental ED-exposed population assessed separately with a Kaplan-Meyer test to evaluate global curve difference. **b**, snout-vent length of F0 individual at metamorphosis from each exposure (n= 34, 38 and 39.) **c**, weight of F0 individual at metamorphosis from each exposure (n= 34, 38 and 39 for control, BaP and TCS parental exposure respectively). **d**, development curves of F0 juvenile female from hatching to sexual maturity. The distributions of F0 individual development times were compared between control populations and each exposed population assessed separately with a Kaplan-Meyer test to evaluate global curve difference The asterisks indicate a significant difference from the control: *, $p < 0.05$ (n= 17, 19 and 23 for control, BaP and TCS parental exposure).

Figure 1

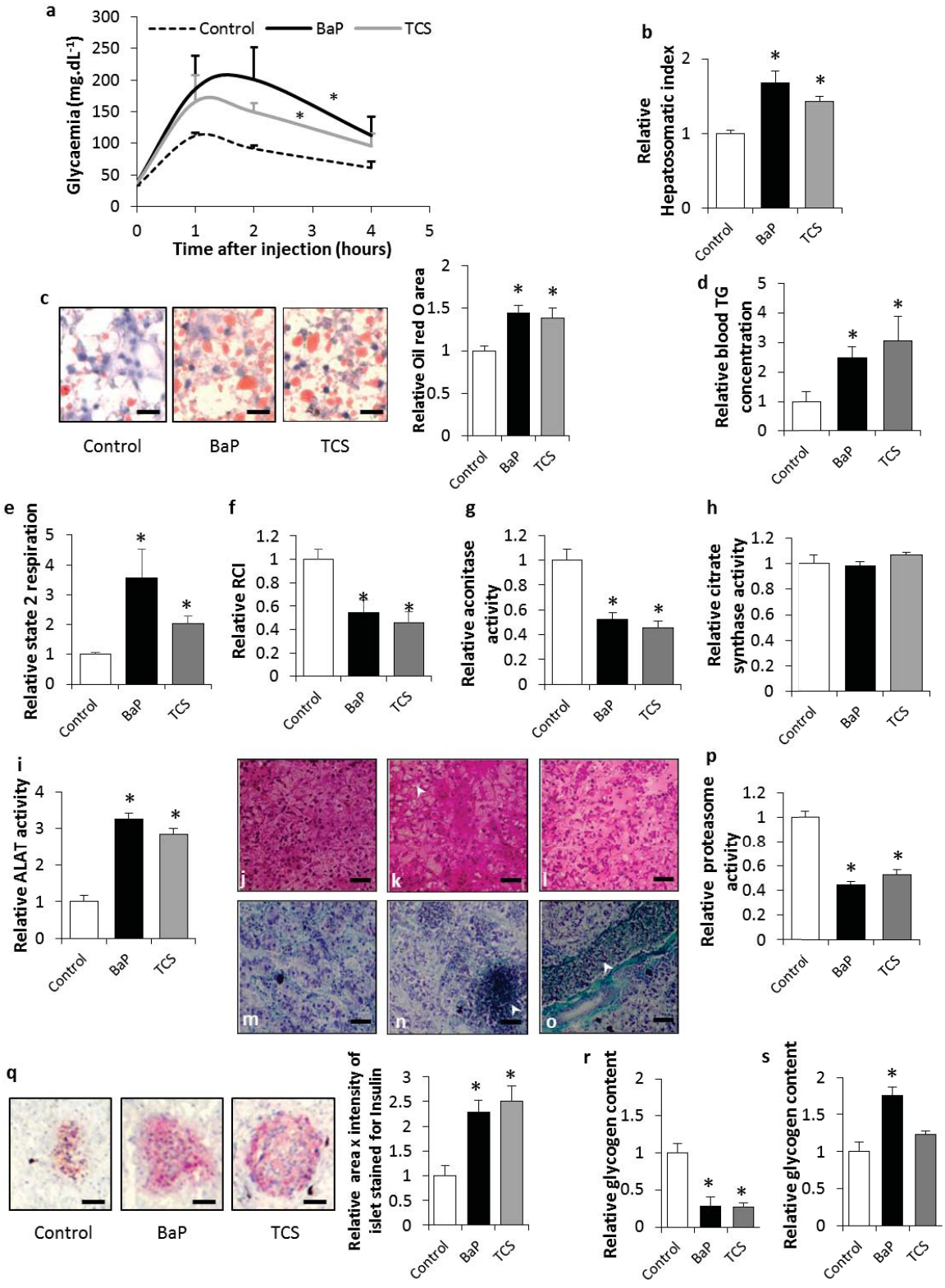
a
Control
BaP
TCS
Glycaemia (mg.dL-1)
Time after injection (hours)
b
Relative Hepatosomatic index
c
Control
BaP
TCS
Relative Oil red O area
d
Relative blood TG concentration
e
Relative state 2 respiration
f
Relative RCI
g
Relative aconitase activity
h
Relative citrate synthase activity
i
Relative ALAT activity
j
k
l
m
n
o
p
Relative proteasome activity
q
Relative area x intensity of islet stained for Insulin
r
Relative glycogen content
s
Relative glycogen content

Figure 2

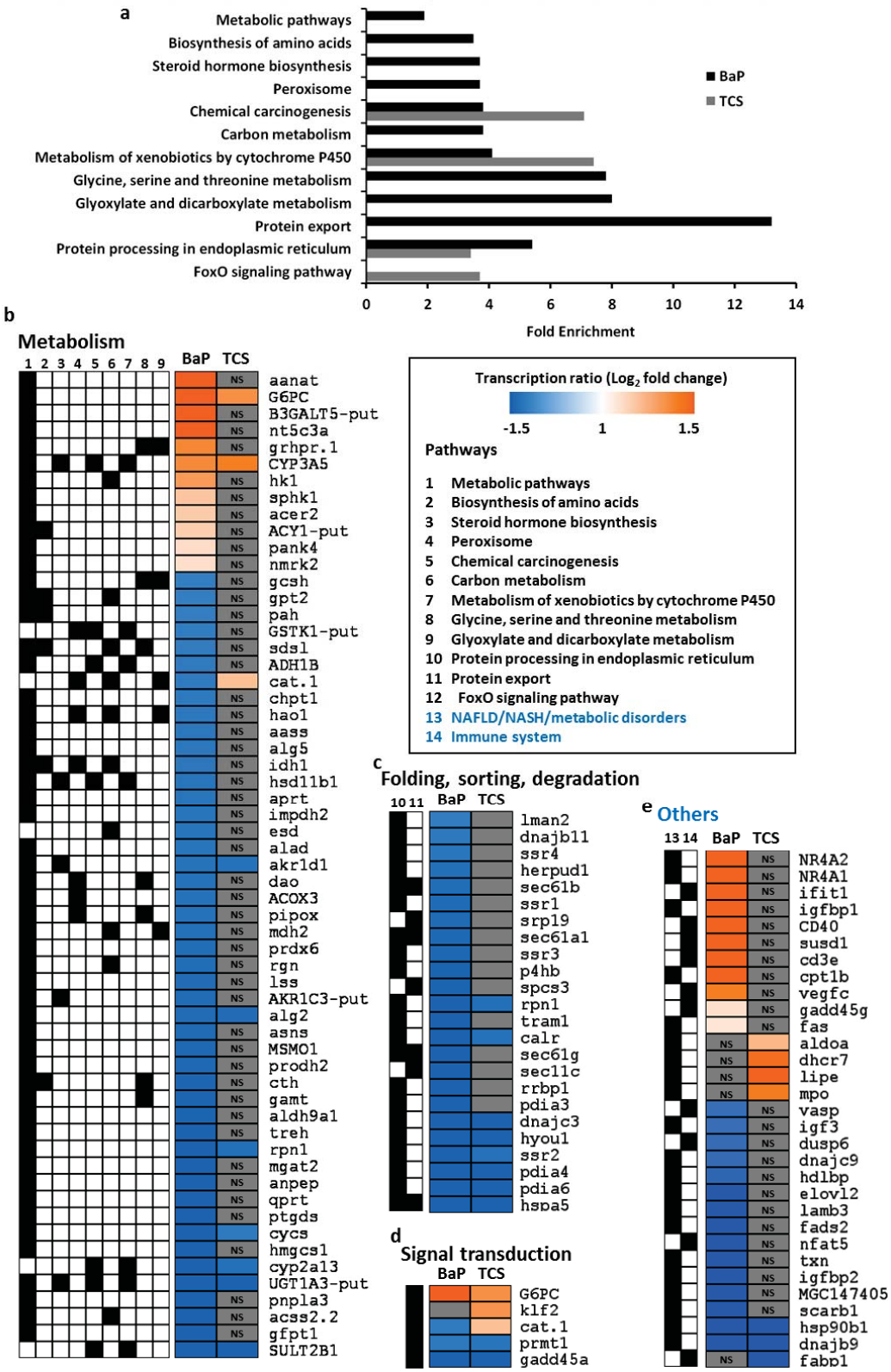
a
Metabolic pathways
Biosynthesis of amino acids
Steroid hormone biosynthesis
Peroxisome
Chemical carcinogenesis
Carbon metabolism
Metabolism of xenobiotics by cytochrome P450
Glycine, serine and threonine metabolism
Glyoxylate and dicarboxylate metabolism
Protein export
Protein processing in endoplasmic reticulum
FoxO signaling pathway
BaP
TCS
0 2 4 6 8 10 12 14
Fold Enrichment
b
Metabolism
1 2 3 4 5 6 7 8 9
BaP TCS
aanat
G6PC
B3GALT5-put
nt5c3a
grhpr.1
CYP3A5
hk1
sphk1
acer2
ACY1-put
pank4
nmrk2
gcsh
gpt2
pah
GSTK1-put
sdsl
ADH1B
cat.1
chpt1
hao1
aass
alg5
idh1
hsd11b1
aprt
impdh2
esd
alad
akr1d1
dao
ACOX3
pipox
mdh2
prdx6
rgn
lss
AKR1C3-put
alg2
asns
MSMO1
prodh2
cth
gamt
aldh9a1
treh
rpn1
mgat2
anpep
qprt
ptgds
cycs
hmgcs1
cyp2a13
UGT1A3-put
pnpla3
acss2.2
gfpt1
SULT2B1
Transcription ratio (Log2 fold change)
-1.5 1 1.5
Pathways
1 Metabolic pathways
2 Biosynthesis of amino acids
3 Steroid hormone biosynthesis
4 Peroxisome
5 Chemical carcinogenesis
6 Carbon metabolism
7 Metabolism of xenobiotics by cytochrome P450
8 Glycine, serine and threonine metabolism
9 Glyoxylate and dicarboxylate metabolism
10 Protein processing in endoplasmic reticulum
11 Protein export
12 FoxO signaling pathway
13 NAFLD/NASH/metabolic disorders
14 Immune system
c
Folding, sorting, degradation
10 11
BaP TCS
lman2
dnajb11
ssr4
herpud1
sec61b
ssr1
srp19
sec61a1
ssr3
p4hb
spcs3
rpn1
tram1
calr
sec61g
sec11c
rrbp1
pdia3
dnajc3
hyou1
ssr2
pdia4
pdia6
hspa5
d
Signal transduction
BaP TCS
G6PC
klf2
cat.1
prmt1
gadd45a
e
Others
13 14
BaP TCS
NR4A2
NR4A1
ifit1
igfbp1
CD40
susd1
cd3e
cpt1b
vegfc
gadd45g
fas
aldoa
dhcr7
lipe
mpo
vasp
igf3
dusp6
dnajc9
hdlbp
elovl2
lamb3
fads2
nfat5
txn
igfbp2
MGC147405
scarb1
hsp90b1
dnajb9
fabp1

Figure 3

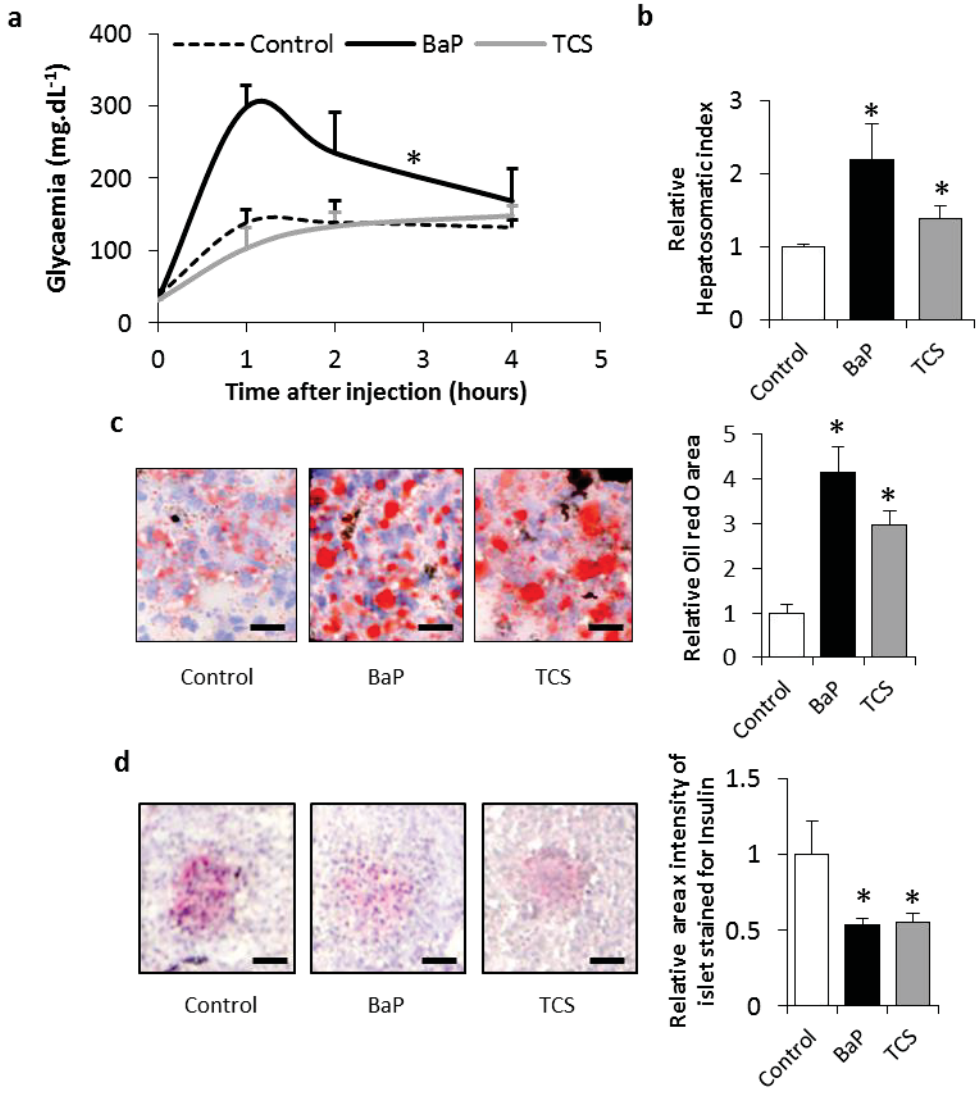
a
Control
BaP
TCS
Glycaemia (mg.dL-1)
Time after injection (hours)
b
Relative Hepatosomatic index
Control
BaP
TCS
c
Control
BaP
TCS
Relative Oil red O area
d
Control
BaP
TCS
Relative area x intensity of islet stained for Insulin

Figure 4

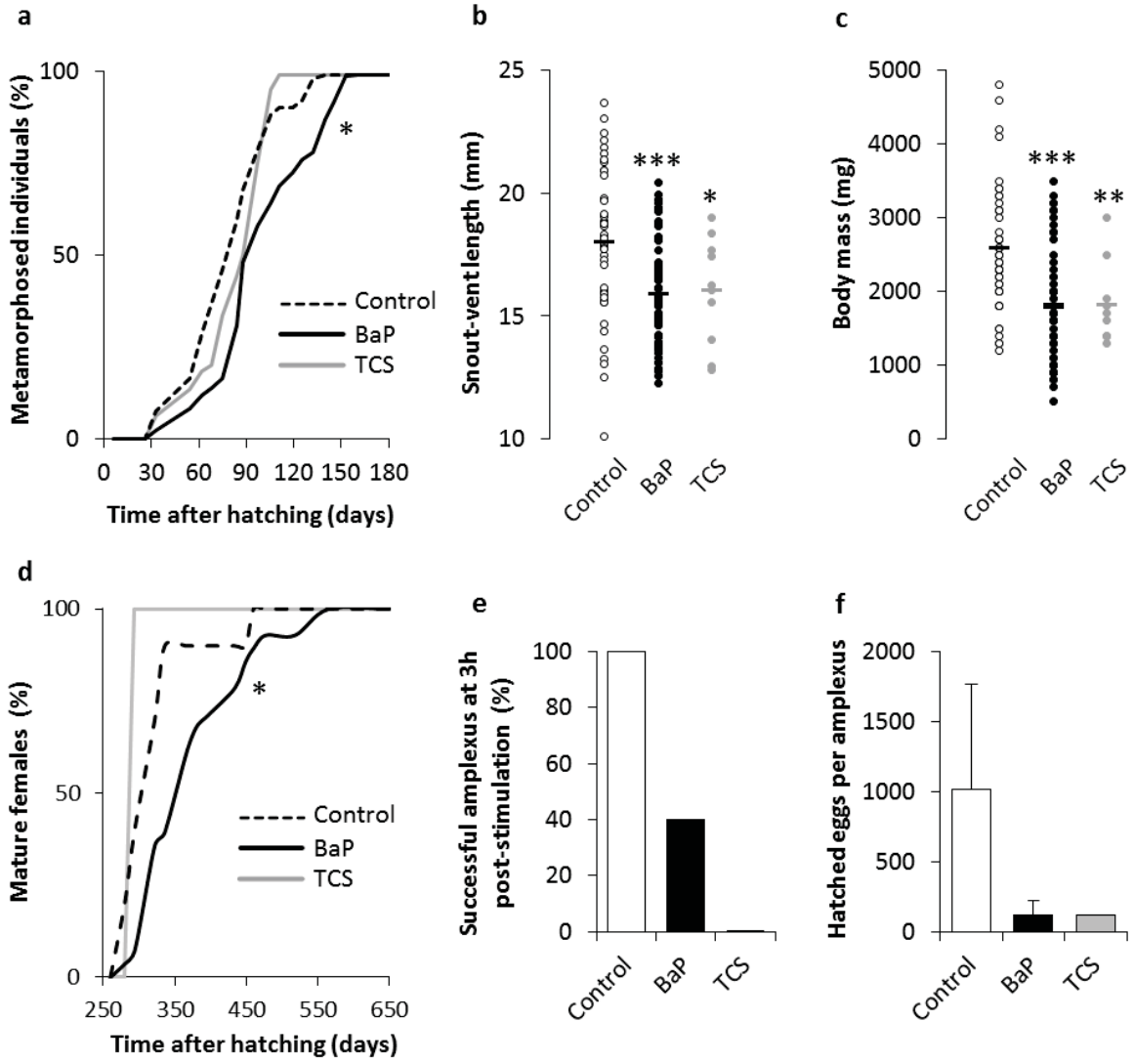
a
Metamorphosed individuals (%)
100
50
0
0 30 60 90 120 150 180
Time after hatching (days)
*
Control
BaP
TCS
b
Snout-vent length (mm)
25
20
15
10
***
*
Control
BaP
TCS
c
Body mass (mg)
5000
4000
3000
2000
1000
0
***
**
Control
BaP
TCS
d
Mature females (%)
100
50
0
250 350 450 550 650
Time after hatching (days)
*
Control
BaP
TCS
e
Successful amplexus at 3h post-stimulation (%)
100
80
60
40
20
0
Control
BaP
TCS
f
Hatched eggs per amplexus
2000
1500
1000
500
0
Control
BaP
TCS

Supplementary Fig 1.